Supporting Information

Geng et al. 10.1073/pnas.1200339109

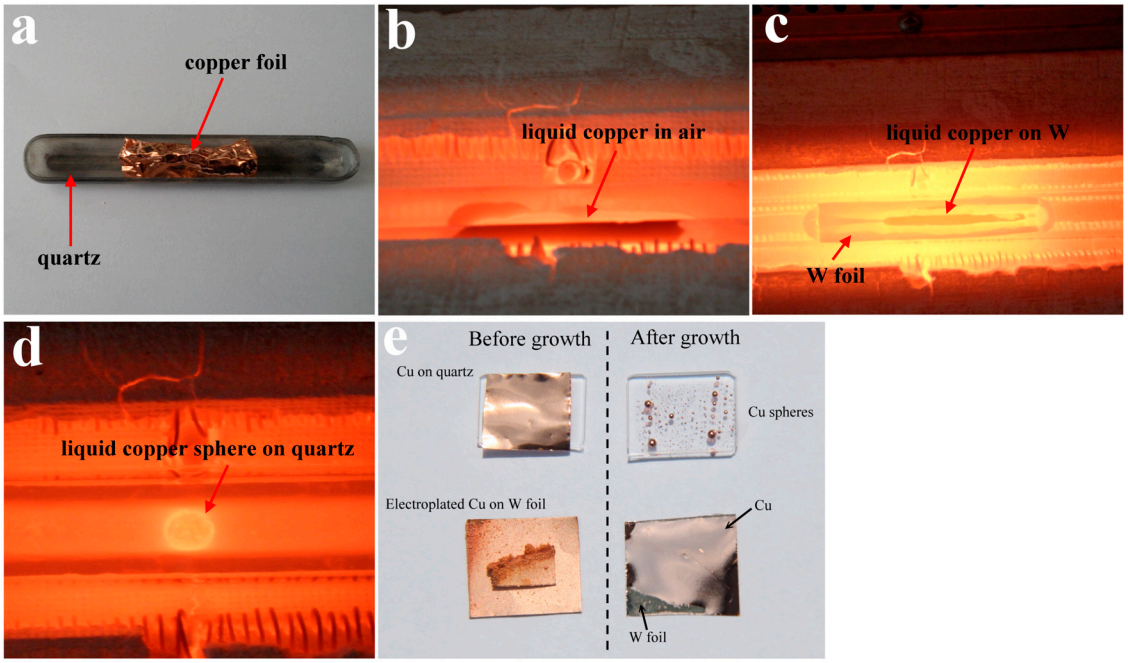

Fig. S1. Evidence for liquid Cu state at growth temperature. Cu foils were first placed in a quartz boat or a W substrate-covered quartz boat. These materials were then heated either in air or in H_2 gas up to 1,100 °C. This temperature was kept for 5–10 min, and then the furnace cover was opened. Finally, the photos were taken at different stages of the process. (*A*) Cu foils in quartz tube before heating; (*B*) the formation of the liquid Cu in air; (*C*) liquid Cu in W/quartz boat; and (*D*) in quartz boat in H_2 flowing conditions, respectively. Liquid Cu state can be clearly seen with naked eyes (*E*). Optical picture showing the morphology changes of Cu on quartz and W substrates before and after graphene growth. Cu foils on quartz were changed to Cu spheres after growth. *Bottom Left* shows electroplated Cu film on W substrates, and Cu film with smooth surface and different morphology was formed after growth. Note that another piece of Cu material produced by electroplating technique was placed onto the electroplated Cu film on W foil, showing that different Cu solid morphology essentially resulted in the similar Cu film after growth. The formation of flat Cu film on W substrate after growth demonstrates their good wetting properties. Note that it is possible for atom diffusion into other matters at Cu/W contact area at high temperature, which accounts for the soldering of two substrates after growth. However, bulk alloying did not happen. No observable changes of morphology occurred to W substrates, and our routine energy dispersive X-ray measurements showed no sign of the existence of substrate elements on Cu surface after growth.

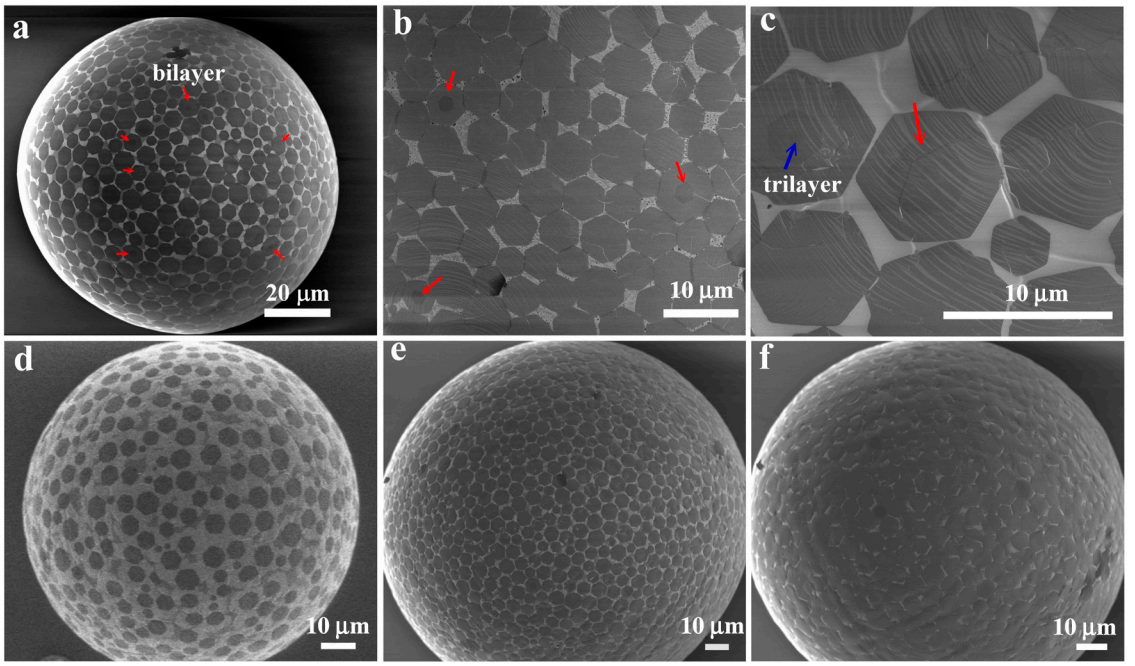

Fig. S2. (*A*–*C*) SEM images with different magnifications of bilayer and trilayer hexagonal graphene flakes (HGFs) formed on liquid Cu spheres. Note that most of the individual HGFs in bilayer or trilayer structures have the same orientation. (*D*) SEM image of HGFs grown on Cu spheres using 10 standard cubic cm per min CH_4 and 300 H_2 for 18 min at 1,080 °C. (*E* and *F*) SEM images of HGFs grown on different Cu spheres with different densities for 20 min.

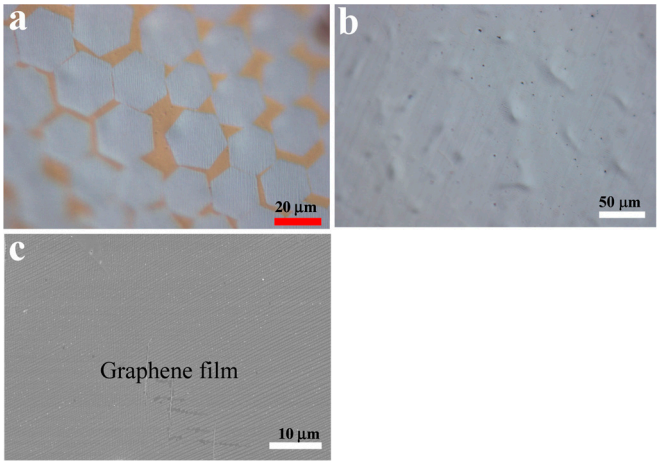

Fig. S3. (*A*) Optical image showing well-dispersed hexagonal graphene flakes (HGFs) grown on flat Cu/W using 6 standard cubic cm per min (sccm) CH_4/300 sccm H_2 at 1,120 °C for 30 min. (*B* and *C*) Optical and SEM images showing continuous film with uniform contrast grown for 2 h with relatively low and high magnification, respectively. Note that the optical image (*B*) of graphene film loses all information on constituted HGF building blocks, showing the formation of continuous film.

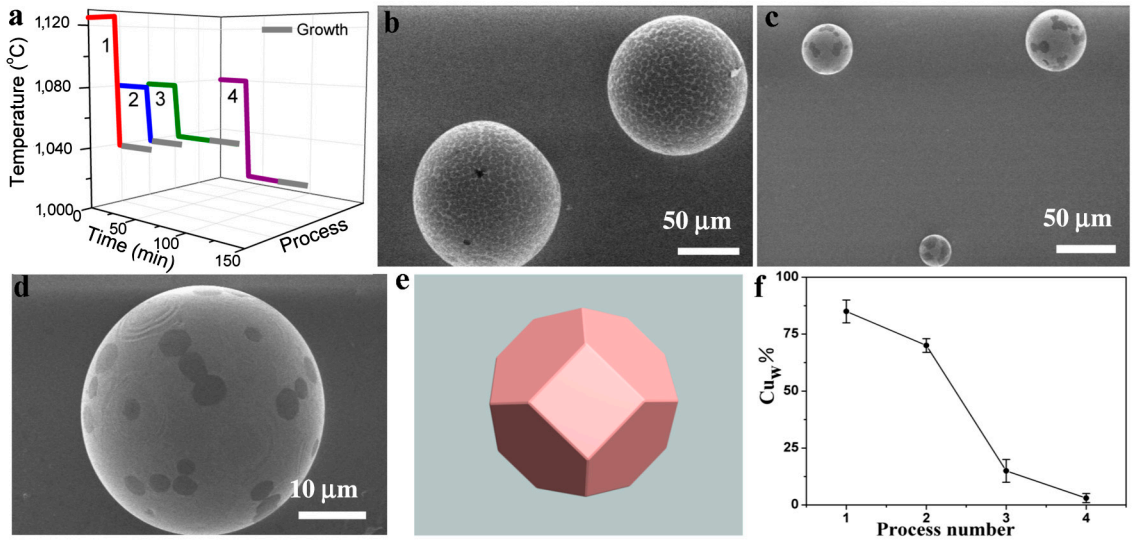

Fig. S4. (*A*) A three-dimensional plot showing the growth processes **1** to **4** with different pregrowth and growth conditions (involving the modulation of initial temperature, annealing time, and reaction temperature). In all cases, 10 standard cubic cm per min CH_4 and 300 H_2 were used for 20 min graphene growth indicated by the gray color bar. Typical SEM images of Cu spheres with (*B*) well-dispersed hexagonal graphene flake (HGF) structures formed in process **1** and (*C*) a nonuniform HGF dispersion obtained using process **4**. Statistical analysis of many SEM images shows that the yield of Cu spheres with well-dispersed HGF structures monotonically decreases from process **1** to process **4**. Note that there are basically two structures of HGF dispersion observed in the experiments. The close-up SEM image (*D*) shows the second kind of structure. Based on geometric considerations, we found that six squares and eight hexagons can perfectly construct this kind of structure by using the Euler equation, as shown in *E*. Cu on the quartz substrate was first melted to form spheres, and then became solid Cu spheres during the lower temperature annealing process during which recrystallization occurred to form Cu polyhedra. Note that HGFs are preferentially grown on the edges of Cu polyhedra. (*F*) A plot of the percentage of Cu spheres with well-dispersed HGFs (Cu_w%) for growth processes **1** to **4**.

The role of the liquid Cu phase in growing well-dispersed HGFs was further revealed by monitoring the yield of Cu spheres as a function of changing Cu surface state. The experiments involved first annealing Cu above its melting temperature for 30 min to form liquid Cu spheres, and then systematically modulating the temperatures and annealing times to change the Cu state from liquid to solid as illustrated in processes **1** to **4** above. These experiments provide a way of studying the correlation between the surface state (i.e., solid or liquid) and the degree of control over layer number and spatial arrangement of HGFs. Processes **1** to **4** represent the increasing tendency of Cu spheres toward conversion to the solid state during the growth process, with Cu spheres existing completely in the liquid state in process **1** and completely in the solid state in process **4** (Fig. S4*A*). It was found that two main structures of HGF ensembles were grown on the Cu spheres, namely well-dispersed HGFs (Fig. S4*B*), and HGFs grown in preferred directions (Fig. S4 *C*–*E*). The latter are possibly related to the formation of Cu crystalline polyhedra by crystallization at temperatures lower than their melting point, resulting in the preferred growth along the edges of Cu polyhedra. A plot of the percentage of Cu spheres with well-dispersed HGFs (Cu_w%) shows a monotonic decrease from process **1** to process **4** (Fig. S4*F*). In the case of process **1**, more than 85% of the Cu spheres had well-dispersed HGFs, and similar results were also obtained by simply growing HGFs at the melting point of bulk Cu (1,080 °C) without lowering the temperature. In contrast, very low values of Cu_w% (~3%) were found in the case of process **4**. The values of Cu_w% for processes **2** and **3** were between those for processes **1** and **4**, possibly reflecting the yield of liquid Cu spheres during each process. These results clearly demonstrate the critical role of liquid Cu as a catalyst for engineering the desired nucleation distribution and spatial arrangement of HGFs.

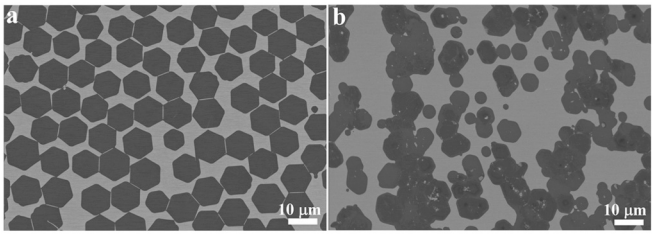

Fig. S5. Control experiment for illustrating role of Cu phase on hexagonal graphene flake (HGF) growth. Briefly, a long strip of Cu foil (~17 cm) on W substrate was used to grow HGFs using 7 standard cubic cm per min (sccm) CH_4/300 sccm H_2 at 1,100 °C for 30 min. Because of temperature gradient, Cu parts away from the central heating zone remained solid though the central Cu strip became liquid at growth temperature. After growth, whether Cu parts were subject to phase change during growth can be easily seen from the appearance. This experiment provides a direct way to compare HGFs grown on liquid and solid Cu in the same run. Typical SEM images were taken on liquid (*A*) and solid (*B*) Cu parts, respectively. This result further confirms the role of liquid Cu in manipulating nucleation, size, and dispersion of HGFs, consistent with the conclusion drawn in the paper.

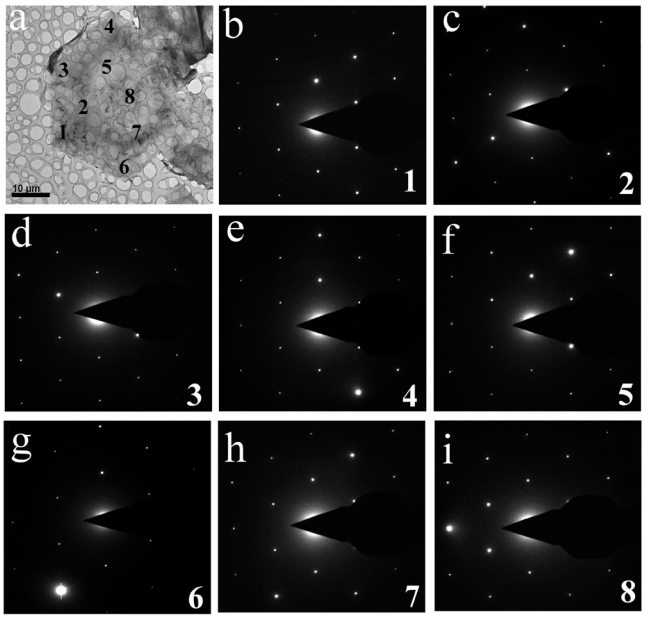

Fig. S6. Transmission electron microscopy (TEM) characterization of the structure of an individual hexagonal graphene flake (HGF). (*A*) Low-magnification TEM image showing an individual HGF. (*B–I*) Selected area electron diffraction (SAED) data for small regions indicated 1 to 8. These SAED data confirm the single crystalline structure of the HGF, as they show the same set of sixfold symmetric diffraction points. The distance between spots 4 and 6 is about 45 μm in this case.

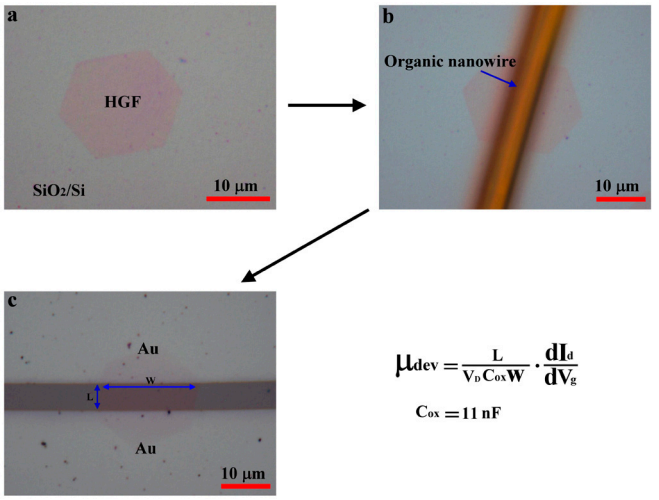

Fig. S7. The procedure for fabrication of hexagonal graphene flake (HGF) field-effect transistor (FET) devices. (*A*) An optical image of an HGF transferred onto 300 nm SiO_2/Si substrate by poly (methyl methacrylate)-assisted method. (*B*) An organic nanowire about 5 μm wide was placed on an HGF with the help of a micromanipulator. (*C*) Approximately 30–40 nm Au film was deposited onto the substrate, and then nanowires were removed by the manipulator. Finally, isolated HGF FET devices were fabricated by scratching Au film. An optical image clearly shows the HGF region after the removal of nanowire. The channel length (L) and width (W) are indicated in the image. Standard FET measurements were carried out on HGF devices, and the extraction of hole mobility is estimated by the equation $\mu_{dev} = \frac{L}{V_D C_{ox} W} \cdot \frac{dI_d}{dV_g}$. The equation and the value of C_{ox} are listed at *Bottom Right*. Other parameters are obtained from device measurements and HGF device dimensions.

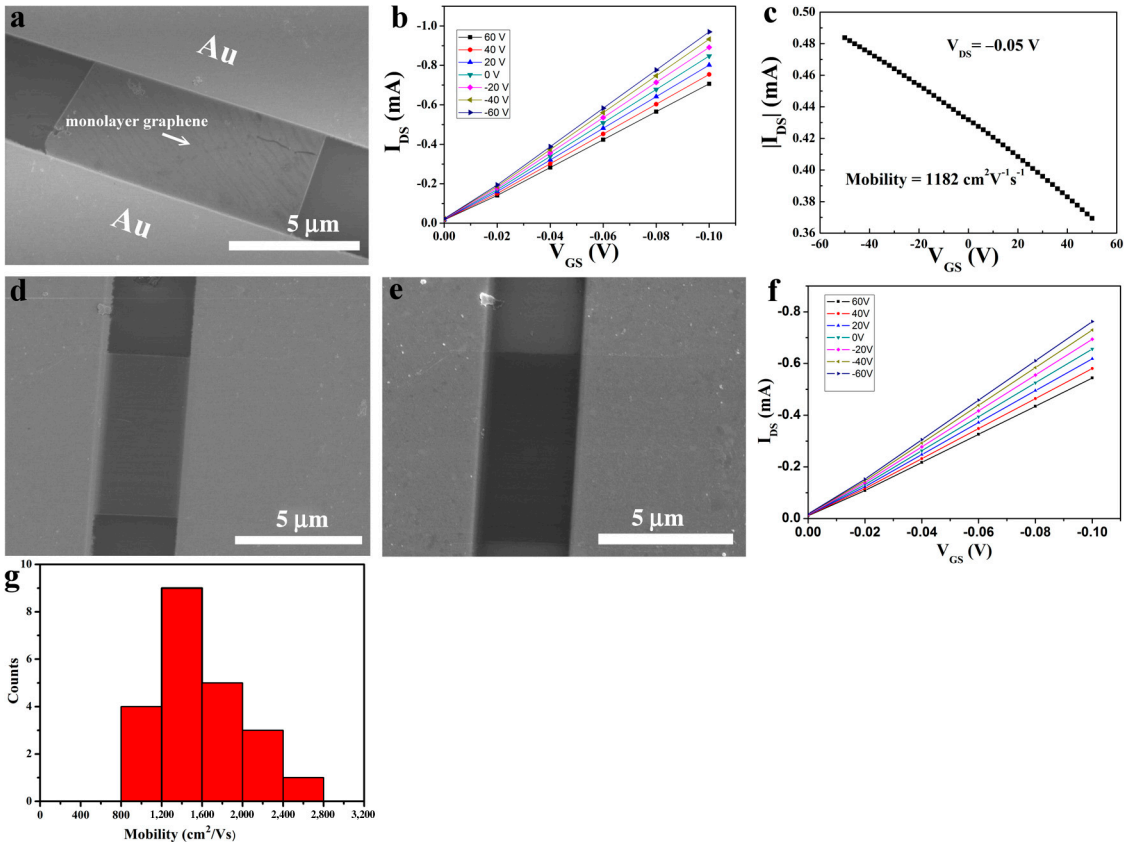

Fig. S8. Electrical measurements of graphene samples transferred onto 300 nm SiO_2/Si substrates. (*A*) SEM image of a field-effect transistor (FET) device based on a monolayer hexagonal graphene flake (HGF). (*B*) Room temperature I_{DS}–V_{DS} characteristics of device (*A*) as a function of V_G in which V_G changes from −60 V (*Top*) to 60 V (*Bottom*). (*C*) The transfer curve for a back-gated FET device (*A*) together with the values of source-drain voltage and derived carrier mobility shown in the *Inset*. Note that the Dirac point was not observed in the range of applied gate voltages measured under ambient conditions, possibly due to oxygen adsorption or doping effects from the transfer process (*D*–*F*). Another example showing device images and the corresponding room temperature I_{DS}–V_{DS} characteristics of the device. Note that SEM images of the same device were taken at acceleration voltages of 1 kV (*D*) and 10 kV (*E*) to show the different contrast of the HGFs. In this case, the resistance at zero gate bias and two-dimensional resistivity were derived from these data to be about 145 Ω and 300 Ω, respectively. Note that the layer number of HGFs in devices of this work was confirmed to be one by optical images and Raman spectra. (*G*) Histogram of hole mobility distribution from 22 HGF devices.

Table S1. Summary of carrier mobility values of graphene or hexagonal graphene flakes grown on solid Cu surface by chemical vapor deposition method from previous work

Device structure	Mobility range (cm^2 V^{-1} s^{-1})	Source
Back-gated	1,000–2,500	This work
Back-gated	1,200–1,971	1
Hall mobility	800–8,000	2
Dual top-gated	4,050	3
Dual top-gated	4,000	4
Back-gated	410	5
Back-gated	2,000–3,000	6
Back-gated	800–7,000	7

Our results are essentially consistent with these main ranges. Note that large scattered data also indicate the complication involved in precise evaluation of carrier mobility.

1. Wu B, et al. (2011) Equilangular hexagon-shape-controlled synthesis of graphene on copper surface. *Adv Mater* 23:3522–3525.
2. Wu W, et al. (2011) Growth of single crystal graphene arrays by locally controlling nucleation on polycrystalline Cu using chemical vapor deposition. *Adv Mater* 23:4898–4903.
3. Li XS, et al. (2009) Large-area synthesis of high-quality and uniform graphene films on copper foils. *Science* 324:1312–1314.
4. Li XS, et al. (2011) Large-area graphene single crystals grown by low-pressure chemical vapor deposition of methane on copper. *J Am Chem Soc* 133:2816–2819.
5. Sun ZZ, et al. (2010) Growth of graphene from solid carbon sources. *Nature* 468:549–552.
6. Ji HX, et al. (2011) Graphene growth using a solid carbon feedstock and hydrogen. *ACS Nano* 5:7656–7661.
7. Li XS, et al. (2010) Graphene films with large domain size by a two-step chemical vapor deposition process. *Nano Lett* 10:4328–4334.